Available online at www.sciencedirect.com
ScienceDirect
Journal of Nuclear Materials 362 (2007) 152–160
journal of nuclear materials
www.elsevier.com/locate/jnucmat

Effect of helium on irradiation-induced hardening of iron: A simulation point of view

R. Schäublin *, Y.L. Chiu [1]

Ecole Polytechnique Fédérale de Lausanne (EPFL), Centre de Recherches en Physique des Plasmas, Association Euratom – Confédération Suisse, 5232 Villigen PSI, Switzerland

Abstract

Irradiation-induced hardening and loss of ductility of ferritic/martensitic materials envisaged for future fusion reactor is still difficult to understand. In particular, helium (He), produced by transmutation by the fusion neutrons of 14 MeV, is known to impact mechanical properties, but its effect at the microstructural level is still unclear. Molecular dynamics simulations of the mobility of an edge dislocation in iron (Fe) are performed to study the effect of He, either as a gas in solid solution or in cavities. Obstacle to the dislocation, the cavity, in the form of a void or a He bubble, is compared to a a_0 [1 0 0] dislocation loop, all being 2 nm in size. Results show that He in solid solution up to 1.0 at.% has a little effect on the dislocation mobility. Conversely, the cavities and the a_0 [1 0 0] dislocation loop are strong obstacles to the passage of the edge dislocation. Interestingly He bubbles present a lower obstacle strength than voids for low He contents, while for high He content the bubble promotes loop punching, which induces a strong resistance to the passage of the dislocation.

PACS: 61.80.Az; 61.72.Ji; 61.72.Lk; 31.15.Qg

1. Introduction

Irradiation-induced defects and transmutation elements produced in the future fusion reactor first wall materials by the impinging 14 MeV fusion neutrons will substantially impact their plasticity. He in particular is known to have detrimental effects on the macroscopic mechanical behaviour of ferritic/martensitic steels [1]. Despite numerous experimental works over several decades, the basic mechanisms underlying these effects are still unclear. The investigation of those by numerical simulations appears nowadays instrumental in expanding our knowledge on this matter. At the basis of this modelization is a hierarchical multiscale approach that encompasses several numerical simulation methods including molecular dynamics (MD) simulations, spanning over many space and time scales. Such an approach substantially increases our ability to predict the long-term behaviour and performance of materials under irradiation.

MD simulations in Fe-based samples of the interaction of a given defect and a dislocation, the vector

* Corresponding author. Tel.: +41 56 310 40 82; fax: +41 56 310 45 29.
E-mail address: robin.schaeublin@psi.ch (R. Schäublin).
[1] Present address: Department of Chemical and Materials Engineering, The University of Auckland, Auckland City, New Zealand.

0022-3115/$ - see front matter
doi:10.1016/j.jnucmat.2007.01.187

of plasticity, are performed to quantify numerically those effects. Nowadays, MD simulations based on the embedded atom method approach [2] allows the investigation at the atomic scale with relatively extended sample sizes. For example, it allows the necessary sample sizes needed to simulate the movement and interaction of a dislocation with structural defects. Previous works, for instance Osetsky and Bacon [3] and Wirth et al. [4] have demonstrated the interaction of a moving dislocation with a void in Fe and with a stacking fault tetrahedron in Cu, respectively, using MD simulations.

In this work, the effect of He on the plasticity of Fe is explored. Firstly, the effect of He in solid solution on the mobility of an edge dislocation in Fe is studied. Secondly, the effect He as a bubble is investigated, and the resulting obstacle strength is deduced. For comparison purposes the effect of a void and a dislocation loop with a Burgers vector a_0 [1 0 0], commonly observed in irradiated ferritic/martensitic steels, is investigated. Finally, the effect of the content of He in the cavity on the mobility of the edge dislocation in Fe is analyzed.

2. Simulation methods

The dislocation is described using anisotropic elasticity of the continuum. It provides a good description of the dislocation down to the core region, as was proven by a comparison with high resolution TEM [5,6]. The formalism of Stroh [7] was selected, as it provides a fairly convenient mathematical description, used successfully in, for example, the weak beam TEM image simulation of dislocations [8]. In this work we derived the code DISLOC. It allows implementing any type of dislocation character, from screw to edge.

MD simulations are performed using the MOLDY code, which was first developed by Finnis [9] and further developed by Diaz de la Rubia and Guinan [10] for the purpose of simulating high-energy displacement cascade. The program uses spherical many-body potentials and the embedded atom method [2]. It uses also the link cell method of Heyes and Smith [11] that allows speeding up the generation of the neighbour list. We modified MOLDY to implement deformation by shear under either constant strain rate or constant stress. In addition, MOLDY was optimized to gain calculation time.

The MD sample is divided in several regions serving different purposes, as illustrated in Fig. 1. The

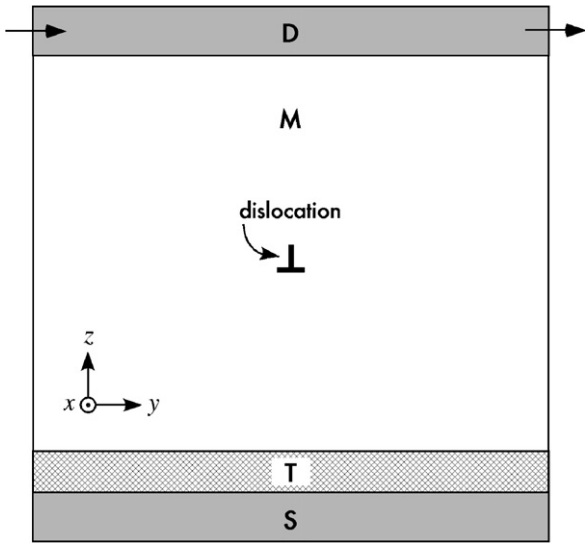

Fig. 1. Schematics of the sample configuration for the dislocation glide as implemented in moldy code, showing the various regions defined for control of the deformation and temperature (details in the text).

dislocation line, along x, is perpendicular to the image plane and moves from left to right, for the case of the edge dislocation. In region M, atoms are mobile following the Newton equations. Periodic boundary conditions apply along x- and y-directions. The upper region D is set to control the deformation of the sample. It is typically 4 lattice units thick and is bounded by a free surface. Under constant strain rate, each atom in D is displaced in the y direction by a fixed increment at each step corresponding to the imposed strain rate. Its speed and acceleration are not calculated. The sum of the forces on each atom in D due to the atoms in M allows deducing the stress response. Under constant stress, each atom in D receives at every time step an additional force in the y direction, which corresponds to the applied stress. Its speed and acceleration are calculated. In region T the temperature is controlled by performing a velocity rescaling on every atom in this region every 100 steps according to the difference between the temperature measured in T and the desired temperature. It implied that the temperature of the sample is controlled by region T, which acts as an infinite thermal bath. Region S contains atoms that are static, implying that their speed and acceleration are not calculated. It allows anchoring the sample, thus avoiding drift in the direction of the applied stress or strain. In the case of a screw dislocation the

imposed stress or strain is applied in the direction of the dislocation line, i.e. along x.

The Fe–He system is described by a combination of interatomic potentials as suggested by Morishita et al. [12]. It is based on the Ackland'97 potential [13], the Wilson–Johnson potential [14] and the Beck potential [15] describing the Fe–Fe, Fe–He and He–He interactions, respectively. The Ackland potential is a many-body type potential that includes the electronic density and an embedding term, while the other two are pair potentials. The Wilson–Johnson potential is purely repulsive and derived from Hartree–Fock–Slater calculations. The Beck potential for He–He interactions was smoothly connected with the Ziegler–Biersack–Littmark universal potential [16] that is appropriate at high energy. One might question the adequacy of these potentials to describe He in a Fe matrix. They give a formation energy of 3.25 eV for a substitutional He atom, while ab initio calculations give 4.22 eV [17]. The formation energy of the most favorable interstitial is 5.34 eV, while ab initio gives 4.39 eV [17]. The most favorable site for a He atom is thus substitutional relative to interstitial, as indicated by both the empirical potentials and ab initio. Moreover, both types of calculations indicate that He shows self-trapping, up to 4 He atoms per vacancy [17]. However, firstly, the magnitude of the difference in formation energy by the empirical potentials is overestimated (2.09 versus 0.17 eV for ab initio) and, secondly, the interstitial site should be tetrahedral, and not octahedral as indicated by the empirical potentials. Nonetheless, these potentials are considered to be appropriate for this work, first of all for the absence of more adequate ones. In addition, the fact that He is a noble gas indicates that no hybridization of He in Fe or charge sharing or exchange can take place. The absence of embedding term in the empirical potential with He allows reproducing this behaviour.

The sample geometry and simulation conditions are the following. An edge dislocation is constructed in a box that is 25 nm long in the dislocation glide direction, 14 nm along the dislocation line and 20 nm thick. The dislocation line is along $[1\,1\,\bar{2}]$ (x direction), its Burgers vector is $1/2\ a_0\,[1\,1\,1]$ (y direction) and its glide plane is $(1\,\bar{1}\,0)$ (z plane). The sample contains about 0.5 million atoms. The defects are a 2 nm cavity or a 2 nm a_0 [1 0 0] loop. They are constructed at 5 nm away from the dislocation to allow for free glide before interaction and are centred on its glide plane. The system containing the dislocation and the defect is relaxed by conjugate gradients prior to deformation. Simulations are performed at 10 K for the sake of visibility of the atomic configurations during the simulation. In effect, as we use the atomic potential energy to select atoms for the display, above about 100 K the thermal noise in the picture makes the identification of the dislocation line difficult. An annealing of 2 ps at 10 K is performed before proceeding to the deformation. Simulations are performed under constant strain rate and the stress response is recorded. The strain rate is quoted as the ratio of the amount of displacement along y of the control layer to the length of the box per time step, which is 1 fs. The stress response in the case of the dislocation interacting with a defect gives the release or escape stress at the moment when the dislocation unpins from the defect, also quoted as the obstacle strength.

3. Results

Fig. 2 shows the resulting flow stress as a function of strain rate at 10 K for an edge dislocation in pure Fe without defects. As expected the flow stress decreases with decreasing strain rate. The stress at the point of yielding, at minute strain levels, indicates the critical stress necessary to move the dislocation. At and below a strain rate value $3.0\times10^{-8}\ \mathrm{fs}^{-1}$ the yield stress saturates, to a value of about 20 MPa. It corresponds to a macroscopic strain rate of $3.0\times10^{7}\ \mathrm{s}^{-1}$ and, for the given sample geometry, to a dislocation speed of $60\ \mathrm{m\ s}^{-1}$. Curves obtained for the strain rates of $3.0\times10^{-9}\ \mathrm{fs}^{-1}$ and $3.0\times10^{-8}\ \mathrm{fs}^{-1}$ are not displayed for the sake of clarity of the graph. The curves for $3.0\times10^{-9}\ \mathrm{fs}^{-1}$ and $1.0\times10^{-8}\ \mathrm{fs}^{-1}$ overlap. It is the value of the Peierls stress, similar to the value obtained by Osetsky et al. under equivalent simulation conditions and geometry [2]. The fluctuations visible in the curves are thermal fluctuations, which frequency in strain increases as the strain rate decreases, or, equivalently, as the dislocation speed decreases. From these results it is concluded that a constant strain rate of $3.0\times10^{-8}\ \mathrm{fs}^{-1}$ is adequate for the simulations.

The dislocation core temperature [18] increases as the dislocation speed increases. Fig. 3 shows the temperature distribution in tone scale in a cross-section of the Fe sample containing the edge dislocation sheared at 10 K and at a strain rate of $10^{-6}\ \mathrm{fs}^{-1}$. Every dot in the picture corresponds to an atom and its tone scale corresponds to its kinetic energy. At this strain rate the dislocation moves at a

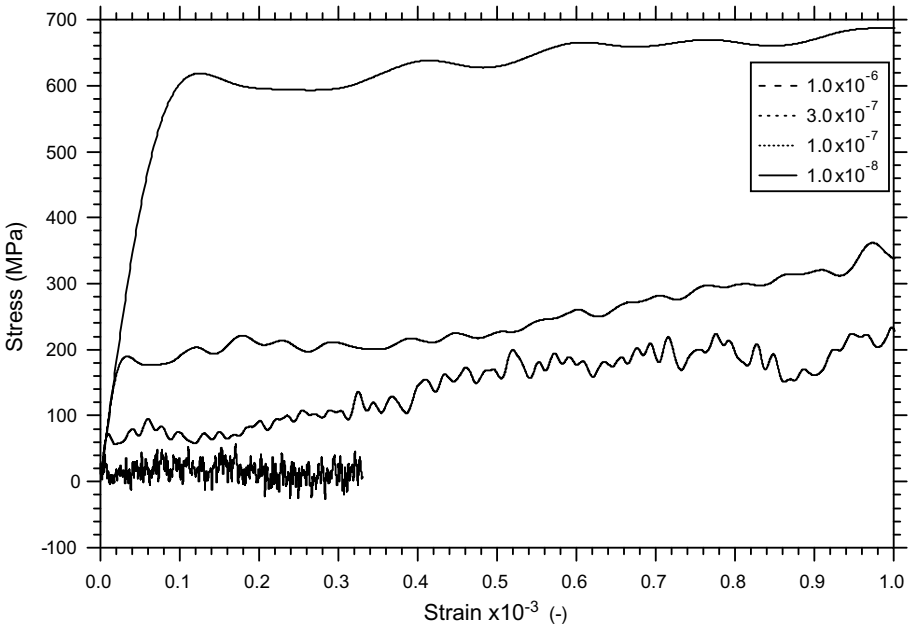

Fig. 2. MD simulated stress as a function of strain rate for an edge dislocation in pure Fe without defects at 10 K. Influence of the strain rate (fs^{-1}).

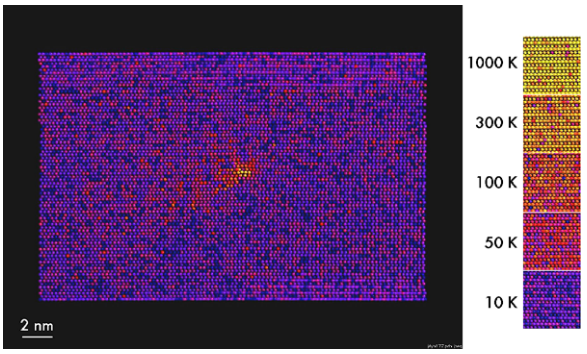

Fig. 3. Cross-sectional view of an MD simulated Fe sample at 10 K containing in the centre an edge dislocation moving from left to right under an imposed strain rate of $1.0 \times 10^{-6}\,fs^{-1}$. Atomic kinetic energy, equivalent to temperature, is represented by the logarithmic tone scale given in the right.

speed of $2\,km\,s^{-1}$, which is the highest speed that the dislocation can reach in this study. It equals approximately the speed of sound in Fe. A dislocation core region of less than 1 nm in diameter reaches temperatures of the order of 1000 K (light region in the centre of the picture), the rest being at 10 K (dark background). In addition, the dislocation, as it travels from left to right in the image, leaves behind a faint hot zone (mid-tone region in the image), which tends to be inclined, relatively to the horizontal line, below the glide plane, and extends over about 5 nm. The hot region relates to regions around the dislocation that are in tension, as opposed to the regions that are in compression, above the glide plane, as the extra plane at the origin of the edge dislocation is pointing upwards in the image. In these simulation conditions and with a specimen without temperature control (insulated sample) the temperature increases by about 68 K after 100 ps, which corresponds to a temperature gradient of $6.8 \times 10^{11}\,K\,s^{-1}$. Note that at $5.0 \times 10^{-7}\,fs^{-1}$ the sample temperature increases by about 2.2 K after 100 ps. For lower strain rates the temperature gradient rapidly decreases to negligible values for the considered simulated times, which reach a maximum of 500 ps. The temperature control is however still necessary in all simulations for those moments when the dislocation escapes from the defect and reaches the highest speeds to avoid uncontrolled heating that can affect its glide.

The influence of He in solid solution on the flow stress of an Fe sample containing an edge dislocation was investigated (Fig. 4). He atoms were placed randomly on Fe lattice sites and the content of He was 0.1 and 1.0 atomic percent. Fig. 4 shows that the presence of substitutional He in the sample does not change significantly the yield stress, even at the highest He content, for two different strain rates,

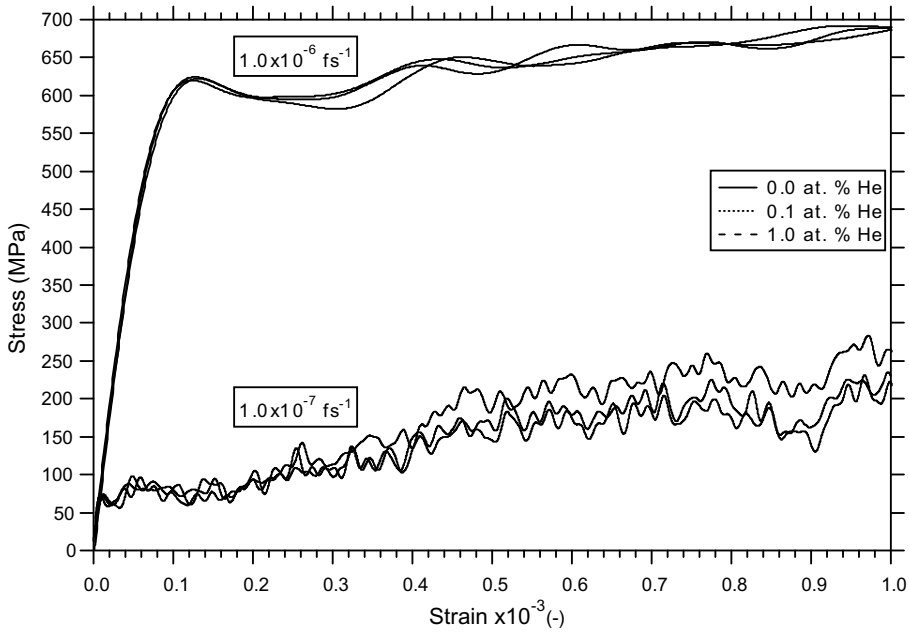

Fig. 4. MD simulated stress response as a function of indicated strain rate and He content of Fe containing an edge dislocation at 10 K.

namely $10^{-6}\,fs^{-1}$ and $10^{-7}\,fs^{-1}$. Only in the flow stress and for the highest He content some differences are observed. For the lowest He content no significant difference is observed.

The obstacle strength presented by a 2 nm defect to a moving edge dislocation in Fe at 10 K was investigated. Fig. 5 shows the difference in stress response with a 2 nm void and a 2 nm a_0 [1 0 0] loop. It shows also the difference in response as a function of the strain rate. It appears that at $3\times10^{-8}\,fs^{-1}$ and below ($1\times10^{-8}\,fs^{-1}$) the response stabilizes, both in terms of release stress and strain. At $1\times10^{-7}\,fs^{-1}$ the general behaviour of the curve is preserved while at $1\times10^{-7}\,fs^{-1}$ it is unpredictable and release stress and strain reach higher values. However, the dislocation–defect interaction morphology is observed to be the same for all investigated strain rates. At low strain rates, the shape of the curve follows the evolution of the dislocation. There is firstly a free movement of the dislocation towards the void, at low flow stress, followed by the attraction of the dislocation to the defect, inducing a drop in flow stress. Then there is pinning, followed by bowing of the dislocation at the void, with a corresponding monotonous increase in flow stress. Finally there is a rapid release of the dislocation, resulting in a sharp decrease in flow stress, and then the dislocation travels fast and meets again the void due to periodic boundary conditions with, again, an increase in flow stress. It appears that the lower the strain rate the sharper the drop in flow stress at the unpinning.

It appears that both the 2 nm void and the 2 nm a_0 [1 0 0] loop are strong obstacles, compared with the He solid solution. The obstacle strength amounts to 590 MPa for the void and to 440 MPa for the a_0 [1 0 0] loop. The void strength is in agreement to what Osetsky and Bacon found with the same potential [20]. The a_0 [1 0 0] loop releases the dislocation sooner than the void, at about half the needed strain. While the increase in flow stress is similar, the amount of work, or energy, to overcome the obstacle is larger for the void than for the loop. Note that the interaction of the dislocation with the a_0 [1 0 0] loop leads to a dislocation reaction implying local changes in the Burgers vector of the impinging dislocation.

Fig. 6, top image, shows view from top the pinning of the dislocation on the void as it bows out and tries to escape from it. Note the two dislocation segments that are pulled out. The right segment is closing the gap to meet the left segment, indicating a higher mobility. The bottom image in Fig. 6, showing the event from the front, indicates that the segments have a screw character as depicted by the three light dots denoting its typical threefold symmetry of screw dislocation [19]. The right segment moves in its twinning direction as opposed

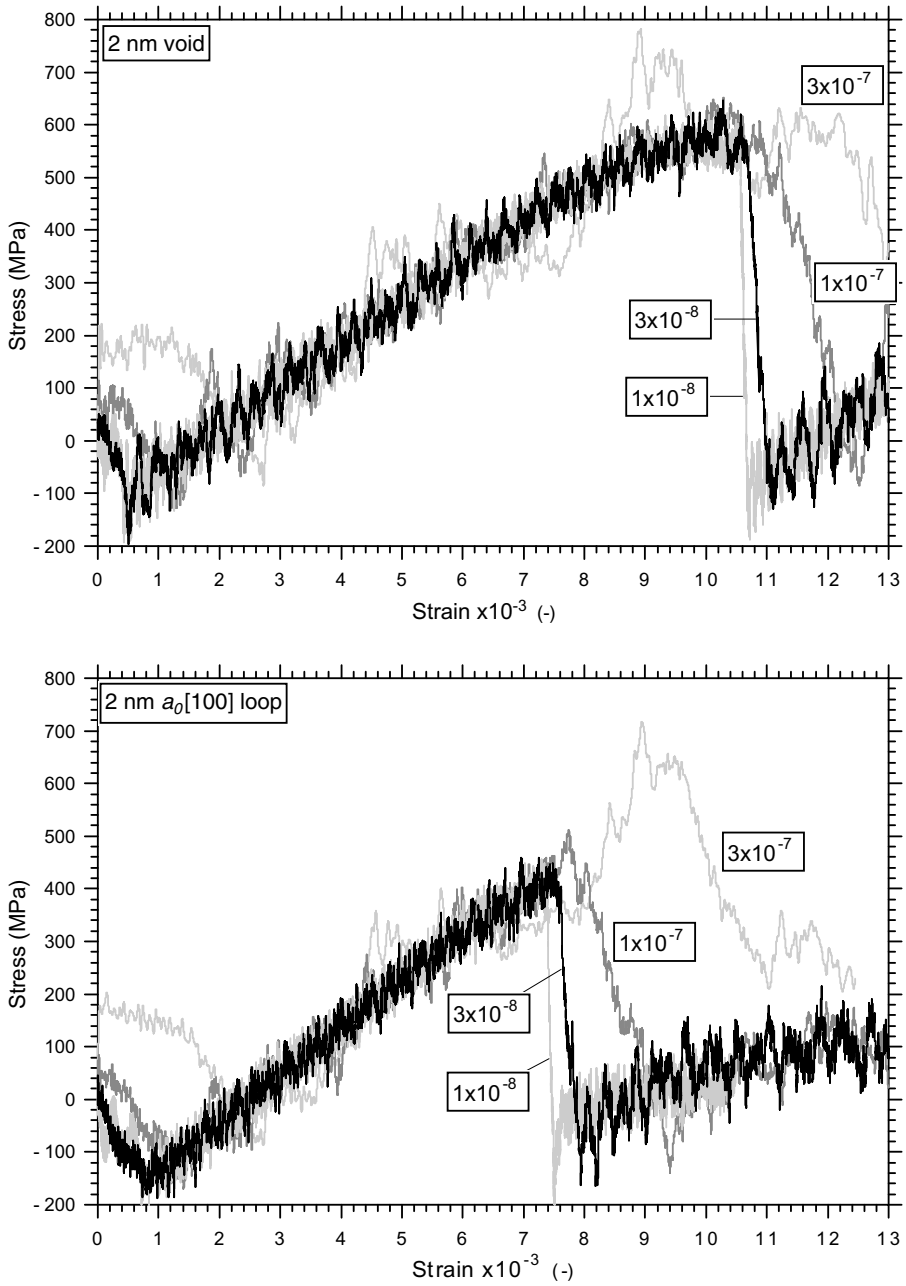

Fig. 5. MD simulated stress response in Fe at 10 K for an edge dislocation interacting with a 2 nm void or a 2 nm a_0 [1 0 0] loop as a function of indicated strain rate (fs^{-1}).

to the left segment that moves in its anti-twinning direction. It explains its higher mobility.

Fig. 7 shows the release stress and strain for a 2 nm cavity at 10 K as a function of the He content, which is given as the number of He atoms per vacancy. It appears that the void is a stronger obstacle than the He bubble at low He contents. The bubble strength decreases with increasing He content up to 2 He atoms per vacancy, where it reaches its weakest condition, giving and obstacle strength of 350 MPa. The release strain is also reduced, to about half the value needed for the void. With more than 2 He atoms per vacancy, the bubble strength and release strain increase with further increase in He content. Note that the He content was increased because of the indications given by ab initio

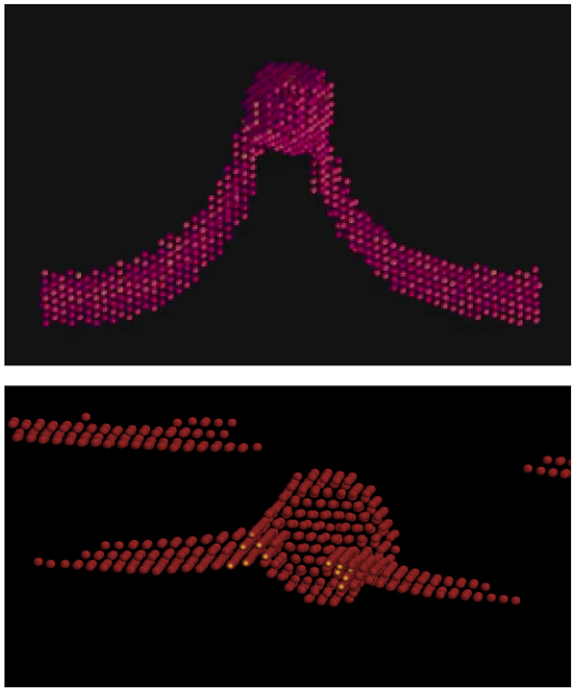

Fig. 6. View of the MD simulated Fe sample containing an edge dislocation line pinned by a 2 nm void as depicted by atoms whose potential energy E_p is higher than −4.28 eV. Top: view in the glide plane showing two dislocation segments being pulled from the void by the escaping dislocation. Bottom: front view, light dots indicate that pulled segments have a screw character with its threefold symmetry.

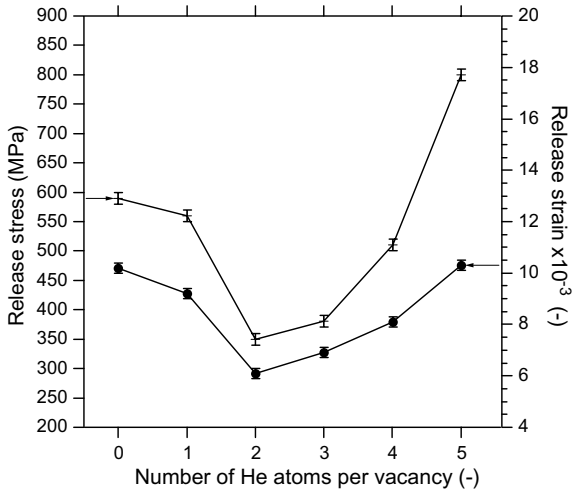

Fig. 7. MD simulated stress and strain response of strained Fe at 10 K containing an edge dislocation interacting with a 2 nm He bubble as a function of the He content in the bubble.

calculations that the stability of a He bubble should increase with He content [17]. At 5 He atoms per vacancy, the obstacle strength of the bubble at 800 MPa overcomes the one of the void.

Fig. 8 shows the snapshots from a sequence of the interaction of an edge dislocation in Fe with a 2 nm He bubble containing 5 He atoms per vacancy. It appears that there is loop punching, in the form of emission of short dislocation segments attached to the cavity, rendering it larger than the original 2 nm sphere. It occurs already during the relaxation of the sample, before straining (Fig. 8(a)). As the dislocation approaches, there is a dislocation reaction that the impinging dislocation (Fig. 8(b)). Finally the dislocation can go through (Fig. 8(c)) and escapes with significant jogs along its line (Fig. 8(c)). More in detail, as the dislocation approaches, the dislocation reaction triggers the formation of a dislocation segment, B, that repels the impinging dislocation, A. This is evidenced in the cross-sectional view in Fig. 8(d), showing segments A and B, and the inside of the He bubble, which is deformed by the internal pressure. The loop punching and subsequent mechanisms explain the extreme obstacle strength presented by this He bubble.

In the literature there is experimental evidence of gas bubble induced loop punching, such as for H bubbles in Cu [21] and He bubbles in Al–0.4Li [22]. While there is indication from ab initio simulations that He in Fe tends to strongly bind with vacancies at least up to 4 He atoms per vacancy [17] and probably more due to the so-called self-trapping of He [23], to our knowledge however there is no experimental observation of such loop punching in ferritic materials. While in the literature there are experimental results indicating hardening due to He, the present simulation work show that the effect of He on plasticity may not be as direct as the ones suggested here. The effect of He may lie on the migration of point defect populations, whereby interstitials and vacancies stabilization in clusters is affected by He, which in turn will modify the density and size of voids, which are strong obstacles. Embrittlement is another effect that could be induced by He, through He segregation to grain boundaries for example, and that would be worth studying by simulations.

4. Summary

Molecular dynamics simulation of the effect of He on the mobility of an edge dislocation in Fe was performed at 10 K. In our simulations the

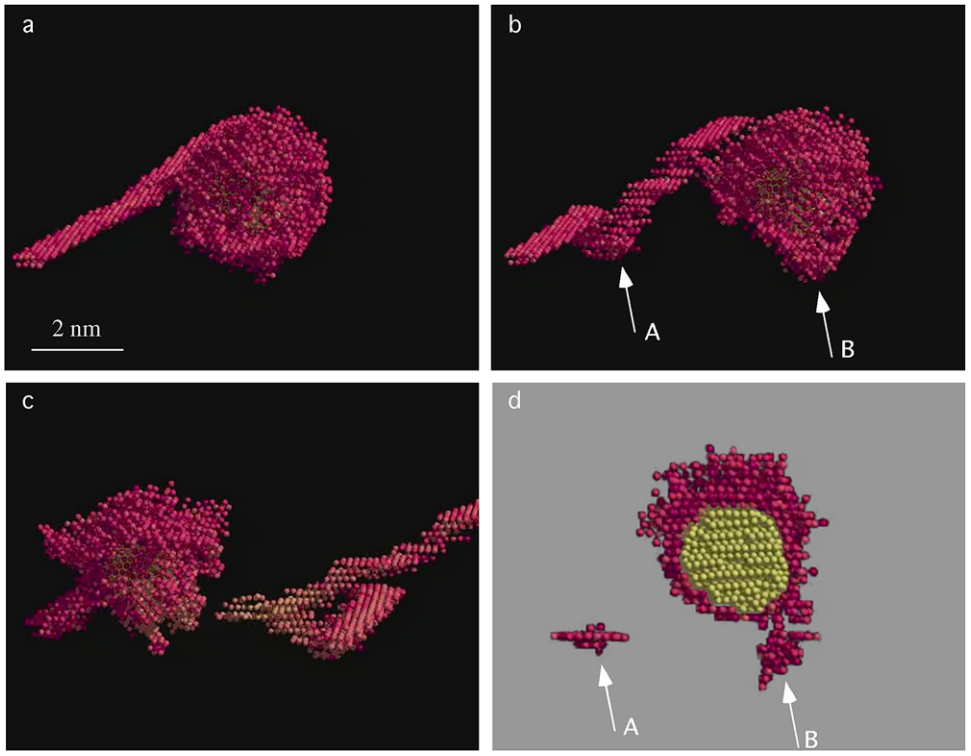

Fig. 8. Four snapshots of the time evolution of the MD simulated interaction in Fe at 10 K of an edge dislocation interacting with a 2 nm He bubble containing 5 He atoms per vacancy (details in text).

Peierls stress for an edge dislocation in pure Fe is about 20 MPa. It appears that He in solid solution has no significant effect on the yield stress. There is some effect on the flow stress at 1.0 at.% He. The 2 nm void presents an obstacle strength of 590 MPa to the edge dislocation. A 2 nm sessile a_0 [1 0 0] loop appears to be also a strong obstacle, at 440 MPa, comparable in obstacle strength to the cavity. A 2 nm He bubble is a weaker obstacle than the 2 nm void when the He content is low, at 1 and 2 He atoms per vacancy. Beyond 2 He atoms per vacancy, a content at which the bubble is the weakest, the resistance of the He bubble increases with increasing He content. At 5 He atoms per vacancy, the He bubble becomes a much stronger obstacle, which is due to significant loop punching.

Acknowledgements

J. Marian, M.J. Caturla, D. Rodney, B. Singh, J. Evans are thanked for fruitful discussions. EFDA is thanked for financial support (task TW3_TTMS_007_D10). The Paul Scherrer Institute is acknowledged for the overall use of the facilities.

References

[1] R. Klueh, D. Harries, High-Chromium Ferritic and Martensitic Steels for Nuclear Applications, American Society for Testing and Materials, West Conshohocken, PA, 2001.
[2] M.S. Daw, M.I. Baskes, Phys. Rev. B 29 (1984) 6443.
[3] Y.N. Osetsky, D.J. Bacon, Model. Simul. Mater. Sci. Eng. 11 (2003) 427.
[4] B.D. Wirth, V.V. Bulatov, T. Diaz de la Rubia, J. Eng. Mater. Technol. – Trans. ASME 124 (3) (2002) 329.
[5] M.J. Mills, P.A. Stadelmann, Philos. Mag. A 60 (1989) 355.
[6] T.J. Balk, K.J. Hemker, Philos. Mag. A 81 (2001) 1507.
[7] A.N. Stroh, Philos. Mag. (1959) 625.
[8] R. Schäublin, P. Stadelmann, Mater. Sci. Eng. A 164 (1993) 373.
[9] M.W. Finnis, MOLDY6 – A Molecular Dynamics Program for Simulation of Pure Metals, Harwell Report AERE-R-13182, 1989.
[10] T. Diaz de la Rubia, M.W. Guinan, J. Nucl. Mater. 174 (1990) 151.
[11] D.M. Heyes, W. Smith, in: Information Quarterly for Computer Simulation of Condensed Phases, No. 26, Science and Engineering Research Council, Daresbury Laboratory, Daresbury, Warrington WA4AD, England, 1987, p. 68.
[12] K. Morishita, R. Sugano, B.D. Wirth, T. Diaz de la Rubia, Nucl. Instrum. and Meth. B 202 (2003) 76.
[13] G.J. Ackland, D.J. Bacon, A.F. Calder, T. Harry, Philos. Mag. A 75 (1997) 713.

[14] W.D. Wilson, R.D. Johnson, Rare gases in metals, in: P.C. Gehlen, J.R. Beeler Jr., R.I. Jaffee (Eds.), Interatomic Potentials and Simulation of Lattice Defects, Plenum, 1972, p. 375.
[15] D.E. Beck, Mol. Phys. 14 (4) (1968) 311.
[16] J.P. Biersack, J.F. Ziegler, Nucl. Instrum. and Meth. 194 (1982) 93.
[17] C.-C. Fu, F. Willaime, Phys. Rev. B 72 (2005) 064117.
[18] J.Th.M. De Hosson, A. Roos, E.D. Metselaar, Philos. Mag. 81 (5) (2001) 1099.
[19] V. Vitek, Philos. Mag. 84 (3–5) (2004) 415.
[20] Y.N. Osetsky, D.J. Bacon, Mater. Sci. Eng. A 400&401 (2005) 374.
[21] W.R. Wampler, T. Schober, B. Lengeler, Philos. Mag. 34 (1) (1976) 129.
[22] K. Shiraishi, A. Hishinuma, Y. Katano, Radiat. Eff. 21 (1974) 161.
[23] W.D. Wislon, C.L. Bisson, M.I. Baskes, Phys. Rev. B 24 (10) (1981) 5616.